Spectrochimica Acta Part A: Molecular and Biomolecular Spectroscopy 256 (2021) 119733

Contents lists available at ScienceDirect

Spectrochimica Acta Part A: Molecular and Biomolecular Spectroscopy

journal homepage: www.elsevier.com/locate/saa

Profiling the interaction of a novel toxic pyruvate dehydrogenase kinase inhibitor with human serum albumin

Xianjiu Liao [a,1], Chunlei Zhu [b,1], Ding Huang [c], Xiaoqing Wen [a], Shao-Lin Zhang [c,*], Yizhong Shen [b,*]

[a] West Guangxi Key Laboratory for Prevention and Treatment of High-Incidence Diseases, Youjiang Medical University for Nationalities, Baise 533000, China
[b] School of Food & Biological Engineering, Hefei University of Technology, Hefei 230009, China
[c] School of Pharmaceutical Sciences, Chongqing University, Chongqing 401331, China

HIGHLIGHTS

- There was significant inner filter effect of **XB-1** on the fluorescence spectra of HSA.
- The **XB-1** bound to HSA mainly *via* hydrogen bond and hydrophobic interactions.
- Binding constants, numbers of binding sites, thermodynamic parameters, and binding distances were calculated.
- **XB-1** caused an obvious change in the conformation structure of HSA.

GRAPHICAL ABSTRACT

The binding information of a novel PDK inhibitor **XB-1** to HSA was systematically demonstrated by spectroscopic approaches and molecular docking under simulative physiological conditions.

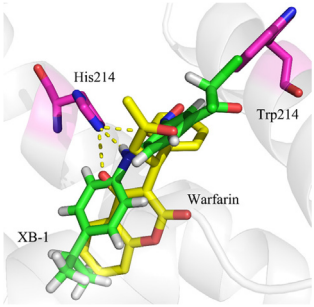

ARTICLE INFO

Article history:
Received 27 November 2020
Received in revised form 16 March 2021
Accepted 18 March 2021
Available online 23 March 2021

Keywords:
Human serum albumin
Molecular docking
Spectroscopic assay
Toxicity

ABSTRACT

To discover novel pyruvate dehydrogenase kinase (PDK) inhibitors, a new compound 2,2-dichloro-1-(4-((4-isopropylphenyl)amino)-3-nitrophenyl)ethan-1-one, namely **XB-1** was identified, which inhibited PDK activity with a half maximal inhibitory concentration (IC_{50}) value of 337.0 nM, and reduced A549 cell proliferation with a half maximal effective concentration (EC_{50}) value of 330.0 nM. However, the compound appears to exhibit a negligible selectivity between cancer cell and normal one, indicating a potential toxicity existed for the compound. Herein, the interaction of the toxic **XB-1** to human serum albumin (HSA) was firstly explored by spectroscopic approaches with the aim to reduce/avoid the toxicity of PDK inhibitors in the next hit-to-lead campaign. In detail, it was found that the **XB-1** could effectively bind to HSA mainly *via* hydrogen bond interaction in PBS buffer (pH = 7.4, 10.0 mM), resulting in the formation of HSA-**XB-1** complex. The negative value of ΔG showed that the binding of **XB-1** to HSA is a spontaneous process. The result from site-selective binding assay suggested that the **XB-1** bound to the site I of HSA by competing with warfarin, which was perfect in agreement with the molecular docking method. The results of this paper may offer a valuable theoretical basis to study the toxicity of biofunctional molecules and may offer thoughts about how to avoid/reduce toxicity for a small molecule.

* Corresponding authors.
E-mail addresses: zhangsl@cqu.edu.cn (S.-L. Zhang), yzshen@hfut.edu.cn (Y. Shen).
[1] X. Liao and C. Zhu contributed equally to this work.

https://doi.org/10.1016/j.saa.2021.119733
1386-1425/

1. Introduction

As we know, it is a simple but useful way to comprehend the potential *in vivo* toxicology of a functional molecule by exploring its binding to plasma protein *in vitro* [1–3]. It is able to do this because the plasma protein plays a significant role in the absorption, transportation, distribution, excretion and metabolism of extraneous chemicals [4–6]. Owing to the excellent carrier function of human serum albumin (HSA) to transport many small molecules *in vivo*, HSA could be regarded as an ideal plasma protein model to predict the potential toxicology, physiological function, and clinical application of small molecules [7,8]. According to previous reports, HSA includes 585 amino acid residues and three homologous α-helical domains (I-III). In each domain, there are two subdomains (A and B) [9,10]. Interestingly, each domain's internal region consists of hydrophobic amino acid residues, while the external region consists of hydrophilic amino acid residues. Moreover, two binding sites (*i.e.*, Sudlow's site I and site II) of extraneous ligands to HSA could be mainly located at the hydrophobic cavities surrounding the subdomains IIA and IIIA [11,12]. Apart from these facts, HSA displays an intrinsic fluorescence, resulting from the sole tryptophan residue (Trp) in the region of Sudlow's site I (Trp-214) [13,14]. Given such unique properties, it is feasible to predict the potential *in vivo* toxicology of endogenous and exogenous ligands/drugs by measuring them triggered the fluorescence change of HSA.

Up to now, a variety of approaches have been exploited to explore the binding behavior of small molecules or ions toward biomolecular proteins, such as equilibrium dialysis [15], potentiometry [16,17], ultraviolet–visible (UV–visible) [18], Fourier transform infrared (FT-IR) [19], circular dichroism (CD) [20], fluorescence spectroscopy [21,22], *etc.* Although equilibrium dialysis has been applied widely, it is time-consuming because it needs the analysis of free and total drug concentration. Meanwhile, potentiometry requires the application of ion selective electrode, easy causing the nonselective drawback in case of many ligands, such as drug molecules. In contrast, UV–visible, fluorescence and CD spectroscopic techniques show the obvious advantages in terms of selectivity, convenience, and short analysis time, which can also obtain the important interaction information of biomolecule protein with small ligand (*e.g.,* ion & small molecule).

Recently, a novel promising PDK inhibitor 2,2-dichloro-1-(4-((4-isopropylphenyl)amino)-3-nitrophenyl)ethan-1-one, namely **XB-1** (molecular structure in Fig. 1) was identified by our efforts [23,24]. The compound exhibited excellent cellular (EC_{50} = 0.33 μM, against A549) and enzymatic activities (IC_{50} = 0.337 μM, PDKs), however, **XB-1** strongly inhibited human normal cells growth (EC_{50} = 0.44 μM, against L02), indicating the compound possess a potential toxicity, which impeded its further pharmaceutical application. To the best of our knowledge, HSA is a plasma protein that plays a curial role in the toxicity/pharmacokinetics of chemicals, which therefore could be employed to predict the potential toxicology, physiological function, and clinical application of small molecules (see Scheme 1).

Inspired by this point, the interaction information of **XB-1** to HSA upon the simulative physiological conditions (PBS, pH = 7.4, 10.0 mM) was examined with the spectroscopic in combination with molecular docking methods, which could be expected to help us to clearly estimate the potential toxicity of **XB-1** *in vivo*. In detail, the binding parameters of **XB-1** to HSA such as fluorescence quenching behavior, thermodynamic information, site-selective binding site, and distance have been investigated in depth.

2. Materials and methods

2.1. Reagents and instruments

All commercial reagents involved in this work were directly bought from the suppliers and no subject to further purification. In detail, human serum albumin (HSA, purity ≥ 99%) was obtained from Yeasen Biotech Co. Ltd. (Shanghai, China). Warfarin (purity > 98%) and ibuprofen (purity ≥ 98%) were acquired from Aladdin Reagent Co. (Shanghai, China). Phosphate buffer solution (PBS, pH = 7.4, 100.0 mM) was bought from KeyGen Biotech. Co. Ltd. (Nanjing, China), which was further diluted with deionized water (D.I. water, resistivity = 18.2 MΩ·cm) to 10.0 mM for uses throughout. Materials for the synthesis of **XB-1** including 4-isopropylaniline, 1-(4-fluorophenyl)ethan-1-one, concentrated nitric acid, concentrated sulfuric acid, 1,3-dichloro-5,5-dimethylhydantoin (DCDMH) were bought from J&K and/or Energy Chemical, which was used without further purification.

UV–visible (UV–vis) absorption spectra were collected on a TU-1901 UV–Vis spectrophotometer (PERSEE, Beijing, China), which was equipped with a 1.0 cm quartz cell. All fluorescence spectra were acquired on a F97pro fluorescence spectrophotometer (Lengguang, Shanghai, China), which was equipped with a thermostat bath as well as a 1.0 cm quartz cell. Fluorescence lifetime curves of HSA in the absence and presence of **XB-1** ($\lambda_{ex}/\lambda_{em}$ = 282 nm/340 nm) were acquired on a FL-TCSPC Fluorolog-3 fluorescence spectrometer (Horiba Jobin Yvon Inc., France). Circular dichroism (CD) spectra of HSA before and after incubation with **XB-1** were measured on a Jasco J-810 Spectropolarimeter (Jasco, Tokyo,

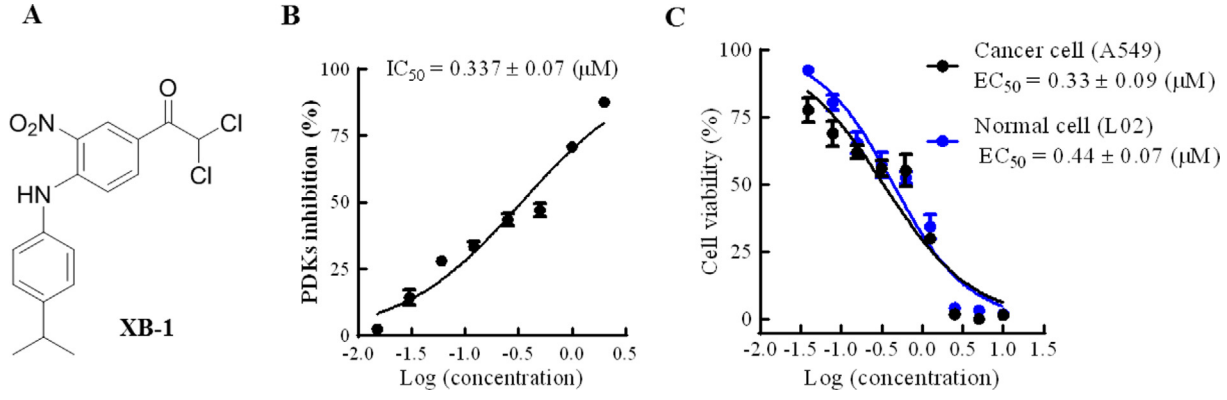

Fig. 1. Biological activities of **XB-1**. (A) Chemical structure of **XB-1**; (B) IC_{50} value of **XB-1** inhibited PDK activity; (C) **XB-1** reduced the growth of cancer cell (A549) and human normal cell (L02).

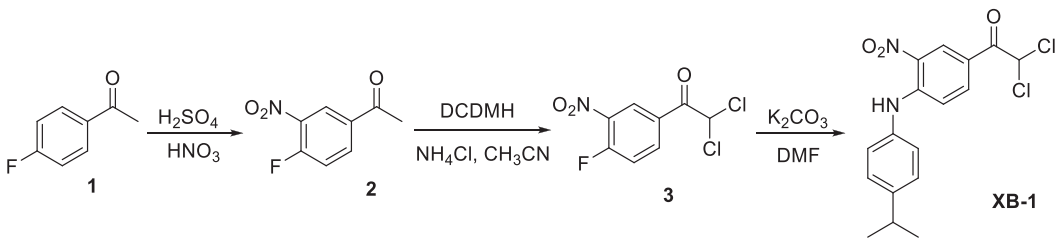

Scheme 1. Synthetic routes for the target compound **XB-1.**

Japan). The reactions were monitored by thin-layer chromatography and carried out on commercial Merck Kieselgel 60 F_{254} plates. Column chromatography was performed on silica gel. ^{1}H NMR spectra were obtained on an Agilent 400 MR spectrometer, while ^{13}C NMR spectra were obtained with proton decoupling on an Agilent 400 MR DD2 (100 MHz). The chemical shifts were reported in parts per million (ppm), the coupling constants (*J*) were expressed in hertz (Hz) and signals were described as singlet (s), doublet (d), triplet (t), as well as multiplet (m). The NMR data was analyzed by MestReNova software. High-resolution mass spectra were obtained on a Bruker SolariX 7.0 T spectrometer. Melting points were recorded on a WRS-2A digital melting point apparatus.

2.2. Synthesis and characterization of XB-1

First, 1-(4-fluorophenyl)ethan-1-one (1) was nitrified in the presence of concentrated nitric acid and sulfuric acid to afford 1-(4-fluoro-3-nitrophenyl)ethan-1-one (2), which was chlorinated in acetonitrile with 2 equivalents of DCDMH at 35 °C for 18 h. Finally, the fluorine group in **3** was then substituted by 4-isopropylaniline to furnish the novel dichloroacetophenone **XB-1**, whose structure was confimed by NMR and HRMS (Figs. S1–S3). M.p. 133–134 °C; ^{1}H NMR (400 MHz, $CDCl_3$): δ (ppm) 9.95 (s, 1H), 9.02 (s, 1H), 8.07–8.04 (m, 1H), 7.35–7.33 (m, 2H), 7.22 (m, 2H), 7.17 (d, *J* = 9.2 Hz, 1H), 6.58 (s, 1H), 3.01–2.94 (m, 1H), 1.29 (d, *J* = 7.2 Hz, 6H); ^{13}C NMR (101 MHz, $CDCl_3$): δ (ppm) 183.29, 148.61, 147.45, 136.03, 134.50, 131.73, 130.37, 128.19, 125.61, 119.72, 116.27, 67.83, 33.94, 24.08. HRMS (ESI): calcd. for $C_{17}H_{15}Cl_2N_2O_3$ $[M-H]^-$: 365.0465, found: 365.0456.

2.3. Fluorescence measurements

In a 1.5 mL PE tube, 10.0 μM HSA and various concentrations of **XB-1** in the range from 0 to 17.0 μM were incubated at the indicated temperature (273 K, 300 K, and 310 K) for 10.0 min. After that, all test sample were applied to acquire the fluorescence spectra upon an excitation wavelength of 280 nm and a scanning wavelength range of 300–500 nm. The excitation and emission slit widths are both 10 nm.

2.4. Absorption and CD measurements

The ultraviolet–visible absorption measurements were performed on the TU-1901 UV–Vis spectrometer with a scan rate of 10 nm/s in the range of 200 nm – 600 nm at 300 K. Absorption spectra were obtained with fixed concentrations of HSA (10.0 μM) and **XB-1** (40.0 μM) in PBS buffer (pH = 7.4, 10.0 mM). For CD measurements, 20.0 μM HSA incubation with 20.0 μM **XB-1** were dissolved with PBS buffer (pH = 7.4, 10.0 mM) in a 1.5 mL PE tube at 300 K for 10.0 min. After that, the two samples were carried out CD measurements in the range of 200–260 nm.

2.5. Molecular docking

Molecular docking was performed using a Sybyl-X 2.0 software. The crystal structure of HSA (PDB code: 2BXD) was downloaded from the Protein Data Bank. The crystal structure of HSA was optimized with H added and charge added by AMBER7 FF99 method. Site I ligand warfarin and site II ligand ibuprofen were selected in PDB files (PDB codes: 2BXD and 2BXG) to generate the protomol by using the software protocols, with the threshold kept at 0.5 and the bloat was fixed as 0. Then structures of small molecules were draw by Sybyl-X 2.0 package, and were subjected to the polar H adding and being energy optimized with a tripos force field and charged optimized with Gasteiger-Huckel method. Finally, molecules were docked to the two main drug binding site I (Subdomain IIA) and site II (Subdomain IIIA) of HSA, respectively. The top 20 preferred conformation of the structure with low energy of the binding system were obtained, and the results with the highest scoring function (Total binding scores) were selected for analysis.

3. Results and discussion

3.1. Profiling the binding of XB-1 to HSA with absorption spectra

In general, the absorption spectra analysis is considered as the simple and straightforward method for profiling the interaction information of a small molecule with biomacromolecule (*e.g.,* serum albumin, and DNA), which could effectively present the alterations of biomacromolecule's structure and surroundings [25]. On this basis, thus, the absorption spectra of HSA-**XB-1** system in PBS buffer (pH = 7.4, 10.0 mM) were firstly examined. As shown in Fig. 2, HSA displayed two distinct absorption peaks at ~217 nm and ~280 nm, respectively. In contrast, **XB-1** showed four absorption peaks at ~228 nm, ~270 nm, ~350 nm, and ~445 nm, respectively. After incubation of **XB-1** with HSA in PBS buffer (pH = 7.4, 10.0 mM), the strong absorption peak of HSA at ~217 nm was red-shifted to ~231 nm, along with an obvious peak intensity decrease. According to previous reports, H_2O, as a polar solvent, possessed a strong capacity to impair the π–π^* transition of C═O in the HSA's polypeptide backbone structure, resulting in the peak intensity decrease of HSA in the range from 200 nm to 220 nm [26,27]. Given such unique feature, when **XB-1** was incubated with HSA in aqueous solution, HSA molecule occurred denaturation and the internal main chain was uncurled, improving the likelihood of encounter between water molecule and the internal amide moieties. As a result, a remarkable decrease of peak intensity as well as an obvious red-shift at this range were observed, demonstrating that **XB-1** could effectively cause the destruction of HSA's secondary or tertiary structure. Additionally, the peak intensity of HSA at ~280 nm was increased and blue-shifted from ~280 nm to ~275 nm, attributable to the remarkable microenvironmental alterations of Trp and Tyr residues in HSA [28]. By subtracting the absorption of **XB-1** from HSA-**XB-1**, there was a hypochromic shift in the absorption peak at ~280 nm by comparing with that of equimolar HSA, probably attributable to the π-π

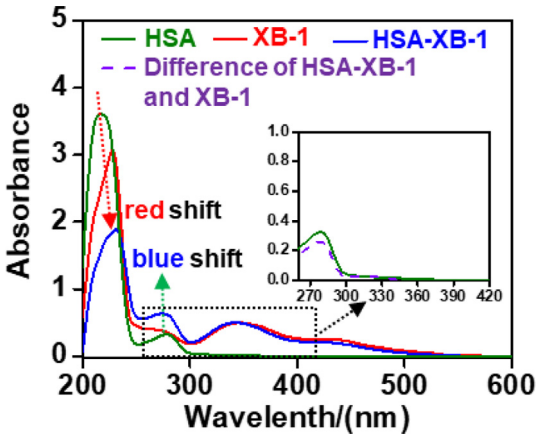

Fig. 2. Profiling the interaction of **XB-1** with HSA in PBS buffer (pH = 7.4, 10.0 mM). Inset: the amplified absorption spectra of HSA and the difference between HSA-XB-1 and XB-1. The concentration of HSA was 10.0 μM, and the concentration of **XB-1** was 40.0 μM.

stacking interaction of **XB-1**'s aromatic ring with the phenyl rings inside HSA amino acid residues [29,30]. In view of these facts, it could speculate that there were strong interactions between **XB-1** and HSA, resulting in a ground-state complex formation (HSA-**XB-1**), foreboding a static fluorescence quenching process of HSA caused by **XB-1** [31–33].

3.2. Fluorescence quenching process

Having confirmed the formation of ground-state complex HSA-**XB-1**, the binding information of **XB-1** to HSA was subsequently examined by a fluorescence assay. As we know, the intrinsic fluorescence feature of HSA could be mainly ascribed to the internal residuals such as tryptophan (Trp), phenylalanine (Phe) and tyrosine (Tyr). Compared with Trp residue, the contribution of Phe and Tyr to the HSA fluorescence emission was almost negligible, resulting from the insignificant fluorescence quantum yield of Phe and the violent fluorescence quenching of Tyr under ionization [34]. Therefore, the fluorescence emission of HSA could be mainly derived from the Trp residues in HSA, which prompted us to set the optimal excitation wavelength at 280 nm for enabling the maximal fluorescence intensity of HSA. By titration of **XB-1** into 10.0 μM HSA, the fluorescence intensity of HSA at ~340 nm was progressively decreased with the concentration increase of **XB-1** in PBS buffer (pH = 7.4, 10.0 mM). Moreover, the maximum emission peak (λ_{max}) was blue-shifted from ~340 nm to ~335 nm, revealing an increased hydrophobicity in the surrounding region of internal Trp residues (Trp-214) (Fig. 3A) [35]. Moreover, owing to the obvious overlapping between **XB-1**'s absorption spectrum and HSA's fluorescence spectrum, the fluorescence spectra of HSA incubation with **XB-1** were corrected for inner filter effect (IFE, Table S1 and Fig. S4) [36,37]. As shown in Fig. 3B, the corrected fluorescence spectra change tendency of HSA incubation with different concentrations of **XB-1** were similar with that of the observed fluorescence spectra. Notably, the corrected fluorescence quenching extent of HSA caused by **XB-1** was smaller than that of the observed result. These findings verified a significant interaction between **XB-1** and HSA in aqueous solution, resulting in obvious fluorescence quenching of HSA, which was consistent with the result of the absorption spectra analysis.

Having calculated the significant corrected fluorescence quenching of HSA after incubation with **XB-1** in PBS buffer (pH = 7.4, 10.0 mM), the classical Stern-Volmer formula (Eq. (1)) was applied to measure the corrected fluorescence quenching constants (K_{sv}) at 273, 300, and 310 K, respectively. By plotting the corrected fluorescence intensity ratio F_0/F versus the concentration of **XB-1**, it could be found that the K_{sv} was inversely proportional to the temperature increase (Fig. 4 and Table 1), demonstrating a static quenching process for corrected HSA fluorescence quenching caused by **XB-1** [38]. To further verify the static quenching process, the fluorescence lifetime curves of HSA before and after incubation with **XB-1** were obtained with a negligible change (Fig. S5), clearly revealing the static process for **XB-1**-triggered the corrected HSA fluorescence quenching [6].

$$F_0/F = 1 + K_{SV}[Q] \quad (1)$$

Among them, F_0 and F corresponded to the corrected fluorescence intensity of HSA at 340 nm before and after incubation with **XB-1**. [Q] expressed the concentration of quencher **XB-1**.

3.3. Exploration of binding and thermodynamic parameters

For a static fluorescence quenching behavior, the binding constant (K_a) of **XB-1** to HSA could be estimated by a modified Stern-Volmer equation (Eq. (2)), which was considered as a powerful tool for intuitively confirming the static quenching process [39]. Based on this consideration, the plotting of $F_0/\Delta F$ versus the reciprocals of different concentrations of **XB-1** ($[Q]^{-1}$) was carried out (Fig. 5A):

$$\frac{F_0}{\Delta F} = \frac{1}{f_a K_a}\frac{1}{[Q]} + \frac{1}{f_a} \quad (2)$$

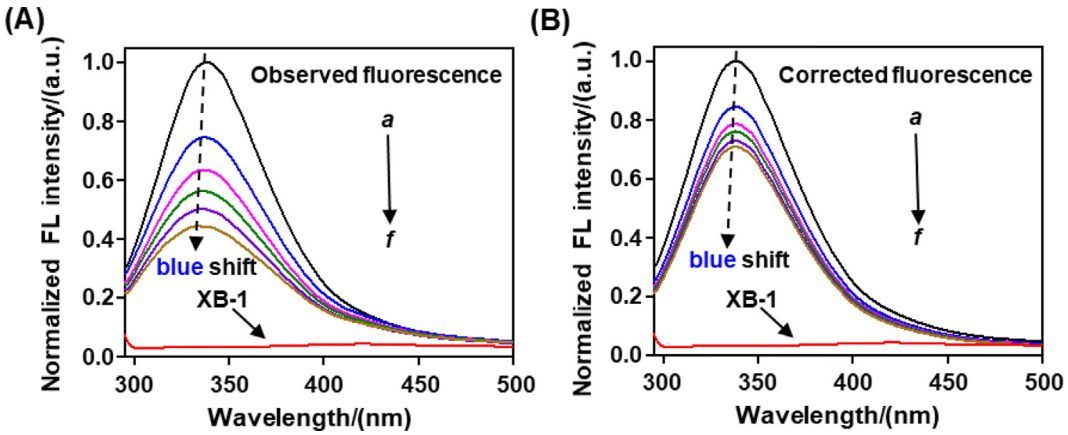

Fig. 3. The (A) observed and (B) corrected fluorescence spectra of 10.0 μM HSA after incubation with **XB-1** at the concentrations from 0.0, 5.0, 8.0, 11.0, 14.0, and 17.0 μM in PBS buffer (pH = 7.4, 10.0 mM), respectively. The concentration of free **XB-1** was 17.0 μM in PBS buffer (pH = 7.4, 10.0 mM). T = 300 K, λ_{ex} = 280 nm.

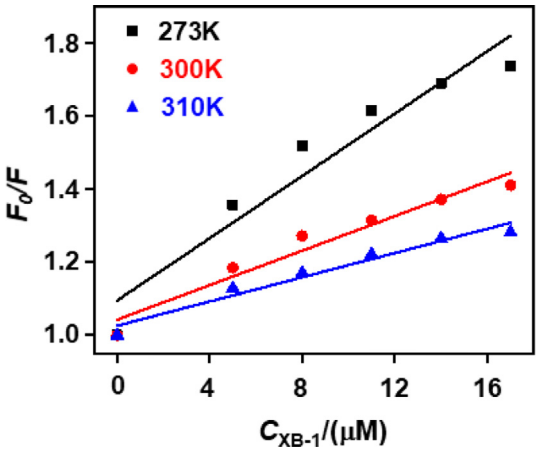

Fig. 4. Stern-Volmer plots for the corrected HSA fluorescence quenching caused by **XB-1** at 273 K, 300 K, and 310 K in PBS buffer (pH = 7.4, 10.0 mM). F_0 and F corresponded to the corrected fluorescence intensity of HSA at 340 nm before and after incubation with **XB-1**.

Table 1
The corrected fluorescence quenching constants (K_{sv}) based on Stern-Volmer equation for the interaction of **XB-1** with HSA at three temperatures of 273 K, 300 K, and 310 K, respectively.

pH	T/(K)	$K_{sv}/(\times 10^4$ L/mol)	r[a]	S.D.[b]
7.4	273	4.26	0.9622	0.06038
	300	2.36	0.9760	0.02636
	310	1.66	0.9806	0.01657

[a] r expressed the correlation coefficient.
[b] *S.D.* expressed the standard deviation for the K_{sv} values.

In this case, ΔF ($\Delta F = F_0 - F$) corresponded to the corrected fluorescence intensity difference of HSA before and after incubation with **XB-1** at different concentration [Q]. In addition, f_a indicated the fractional maximum fluorescence intensity of HSA summed up.

According to the plotting results of $F_0/\Delta F$ versus the concentration reciprocals of **XB-1** at three different temperatures (273, 300, and 310 K), it was found that $F_0/\Delta F$ was positively to the increase of $[Q]^{-1}$, when fixed $(f_a K_a)^{-1}$ as the scope and $(f_a)^{-1}$ as the intercept. In this case, the binding constant K_a could be acquired by performing intercept $(f_a)^{-1}$ to divide the slope $(f_a K_a)^{-1}$, and the results were showed in Table 2.

By report, HSA as a representative serum albumin, displayed multiple sites to bind with extraneous small molecules [5]. Next, the convinced Scatchard equation (Eq. (3)) was applied to examine the number of binding sites (n) for the interaction between **XB-1** and HSA at three different temperatures (273, 300, and 310 K). Moreover, in this case, the equilibrium binding constant (K_b) of the HSA-**XB-1** system at these indicated temperatures could be also achieved [6].

$$r/D_f = nK_b - rK_b \tag{3}$$

In this equation, D_f assigned to the molar concentration of **XB-1**, and r assigned to the moles of **XB-1** that bound to per mole of HSA, which could be calculated with the corrected $\Delta F/F_0$. Moreover, n and K_b assigned to the number of binding sites and the equilibrium binding constant for HSA-**XB-1** system, respectively.

As illustrated in Fig. 5B and Table 2, the K_b in HSA-**XB-1** system could be decreased along with the temperature increase, which was similar to the tendency of temperature effects on K_a above, demonstrating that the binding of **XB-1** to HSA was dependence on incubation temperature. Notably, the number of binding sites (n) between **XB-1** and HSA was less than 1 at 273, 300, and 310 K, suggesting high affinity ability of **XB-1** to HSA. Besides, the K_a at these indicated temperatures were remarkably changed, which was meaningful to a significant temperature effect on the interaction of **XB-1** to HSA in aqueous solution (PBS, pH = 7.4, 10.0 mM). In view of these facts, it might be feasible to apply HSA as an efficient carrier and storage for **XB-1** *in vivo*.

Considering the dependence of K_a on the incubation temperature, the thermodynamic parameters of **XB-1** binding with HSA in PBS buffer (pH = 7.4, 10.0 mM) were measured as well. Usually, the thermodynamic enthalpy change (ΔH) in the binding process between small molecule and serum albumin could be regarded as a constant when the incubation temperature did not remarkably change. In this case, the famous Van't Hoff equation (Eq. (4)) was applied to estimate the relevant thermodynamic enthalpy change (ΔH) and entropy change (ΔS) of the HSA-**XB-1** system:

$$\ln K_a = -\frac{\Delta H}{RT} + \frac{\Delta S}{R} \tag{4}$$

$$\Delta G = \Delta H - T\Delta S \tag{5}$$

Among this equation, R indicated the gas constant (8.314 $J{\cdot}K^{-1}{\cdot}mol^{-1}$), and K_a expressed the binding constant mentioned in Eq. (2). On this basis, a curve of $\ln K_a$ versus $(T)^{-1}$ was fitted by exploiting the K_a values at the temperature of 273, 300, and 310 K. As shown in Fig. 6, the curve's slope and intercept could

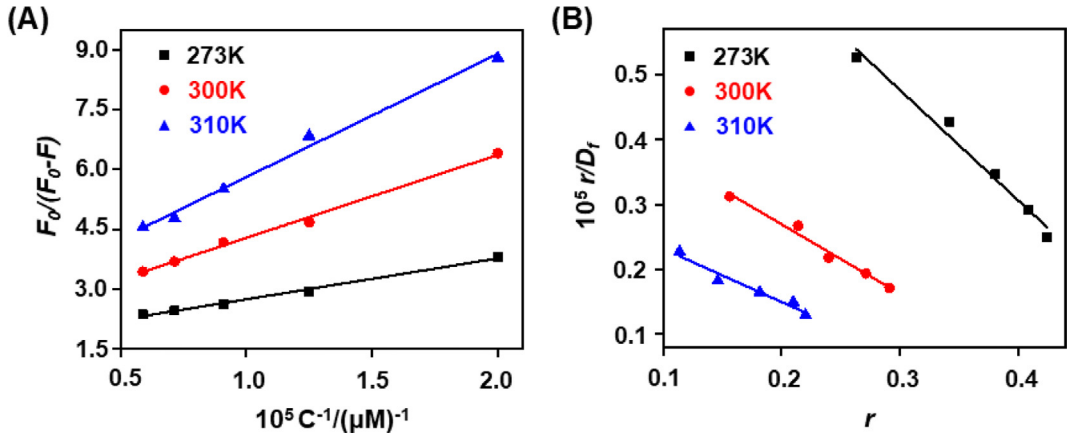

Fig. 5. (A) Modified Stern-Volmer plots and (B) Scatchard plots for the corrected HSA fluorescence quenching caused by **XB-1** at 273 K, 300 K, and 310 K in PBS buffer (pH = 7.4, 10.0 mM).

Table 2
The binding constants and thermodynamic parameters from the fluorescence assay for HSA-**XB-1** system in PBS buffer (pH = 7.4, 10.0 mM).

T (K)	Modified Stern-Volmer Method		Scatchard Method			ΔH (kJ·mol^{-1})	ΔS (J·mol^{-1}·K^{-1})	ΔG (kJ·mol^{-1})
	$10^5 K_a$ (L/mol)	r[a]	$10^5 K_b$ (L/mol)	r[a]	n			
273	1.659	0.9969	1.700	0.9899	0.58			−27.29
300	1.056	0.9978	1.067	0.9896	0.45	−11.98	56.07	−28.80
310	0.874	0.9958	0.818	0.9769	0.38			−29.36

[a] r expressed the correlation coefficient of K_a and K_b values at the temperature of 273, 300, and 310 K, respectively.

be used to achieve the enthalpy change (ΔH) and entropy change (ΔS) of HSA-**XB-1** system, respectively. In combination with the relationship of free energy change (ΔG) with ΔH and ΔS (Eq. (5)), the ΔG of HSA-**XB-1** system at the indicated temperature could be continually calculated, and the corresponding results were summarized in Table 2.

It could be seen from Table 2 that the ΔG values of HSA-**XB-1** system at three temperatures were negative, indicating that the binding of **XB-1** to HSA was spontaneous. Moreover, the negative ΔH value could be ascribed to the hydrogen bonding in this interaction, and the positive ΔS value implied the contributions of hydrophobic interactions in the assembly of ground-state HSA-**XB-1** complex, but the electrostatic interaction could not be ruled out [40].

3.4. Site-selective binding of XB-1 to HSA

Encouraged by the results above, the specific binding site of **XB-1** to HSA was further analyzed. Two distinguished site marker probes (*i.e.* warfarin and ibuprofen) were utilized to perform the site marker competitive experiments, which could accurately reveal the binding site or region of **XB-1** to HSA [6]. According to the principle of competitive experiments, warfarin has been regarded as a specific ligand to primarily bind to the Sudlow's site I located in Subdomain IIA. By contrast, ibuprofen has been considered as another selective ligand to bind to Sudlow's site II located in Subdomain IIIA. As shown in Fig. 7A and B, warfarin could cause obvious corrected fluorescence quenching of HSA, companied with a clear red shift in the maximum emission peak of HSA. This finding demonstrated that there was a remarkable increased polar of the Trp (Trp-214) site region, implying that the binding of **XB-1** to HSA could be interfered by extraneous warfarin. In contrast, ibuprofen displayed a much weaker effect on the corrected fluorescence emission of HSA. Moreover, after addition of ibuprofen, the corrected fluorescence emission of HSA-**XB-1** system was highly similar to that lacking of ibuprofen, suggesting a negligible interference of ibuprofen to disturb the binding of **XB-1** in its usual binding location.

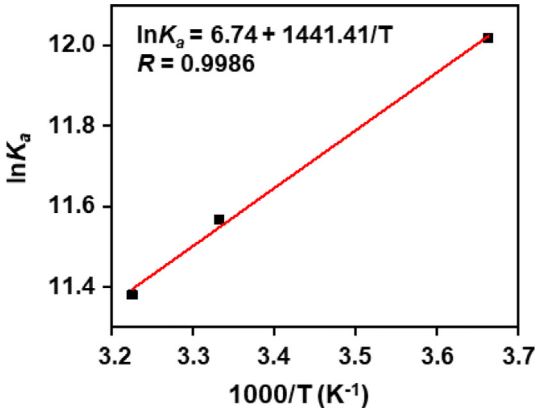

Fig. 6. Van't Hoff plot for the binding of **XB-1** with HSA.

To intuitively compare the interference of warfarin and ibuprofen on the binding of **XB-1** to HSA, in the presence of site markers, the modified Stern-Volmer (Fig. 7C) and Scatchard (Fig. 7D) equations were applied to analyze the binding constant K_a and the equilibrium binding constant K_b. The corresponding results illustrated that the K_a of **XB-1** to HSA was remarkably decreased before and after incubation with warfarin, while ibuprofen showed more moderate interference on the K_a of **XB-1** to HSA (Table 3). Based on these findings, it could be convinced that the binding site of **XB-1** to HSA was occurred at the region surrounding of site I (subdomain IIA) of HSA.

3.5. Molecular docking of XB-1 to HSA

To further verify the binding site of **XB-1** in HSA, **XB-1** was therefore docked into the two main drug binding site I (Subdomain IIA) and site II (Subdomain IIIA), respectively. As shown in Fig. 8, the ligand warfarin located in site I of HSA, where nearby the amino acid of Trp214, and forming direct hydrogen bonding interactions with the Arg222, His242, and Tyr150 [41]. Meanwhile, warfarin exhibited hydrophobic interactions with Trp214, Leu260, Leu238, Ala291, Phe211 in HSA. The **XB-1** showed a very high total binding scores when was docked to the site I (warfarin) of HSA, while the low total binding scores and physical hindrance in site II led us to believe that **XB-1** bound to the site I of HSA. The **XB-1** bound to the Subdomain IIA to form a complex, which was stabilized by the hydrogen bond interactions with Arg218 and His242. Moreover, the hydrophobic interactions were involved in the binding process, which were in perfect agreement with our site-selective binding assay. All these observations indicated that **XB-1** bound to the site I of HSA, and competed with the warfarin to bind to the in site I of HSA, resulting the decrease of K_a/K_b values while binding to HSA. Finally, the complex of HSA-warfarin and HSA-**XB-1** (Fig. 9) was overlapped, finding that the warfarin and **XB-1** was well overlapped and competively bind with His242 in the site I of HSA.

3.6. Profiling of the binding distance

Having revealed the binding site of **XB-1** to HSA, the binding distance of **XB-1** with the internal Trp residuals of HSA was then evaluated. For a binding of small molecule to HSA system, the fluorescence resonance energy transfer (FRET) could be regarded as a powerful method to measure the binding distance between small molecule and the internal Trp residuals of HSA [3]. Usually, it was very necessary to facilitate the energy "donor–acceptor" pair in a close distance (~1–10 nm) for FRET occurrence. In the macroscopical view, the effective spectral overlap of donor's fluorescence spectrum with acceptor's absorption spectrum indicated a FRET process to occur. As demonstrated in Fig. 10, there was a well overlap between HSA's fluorescence emission and **XB-1**'s absorption spectra, suggesting an efficient FRET process in the assembly of

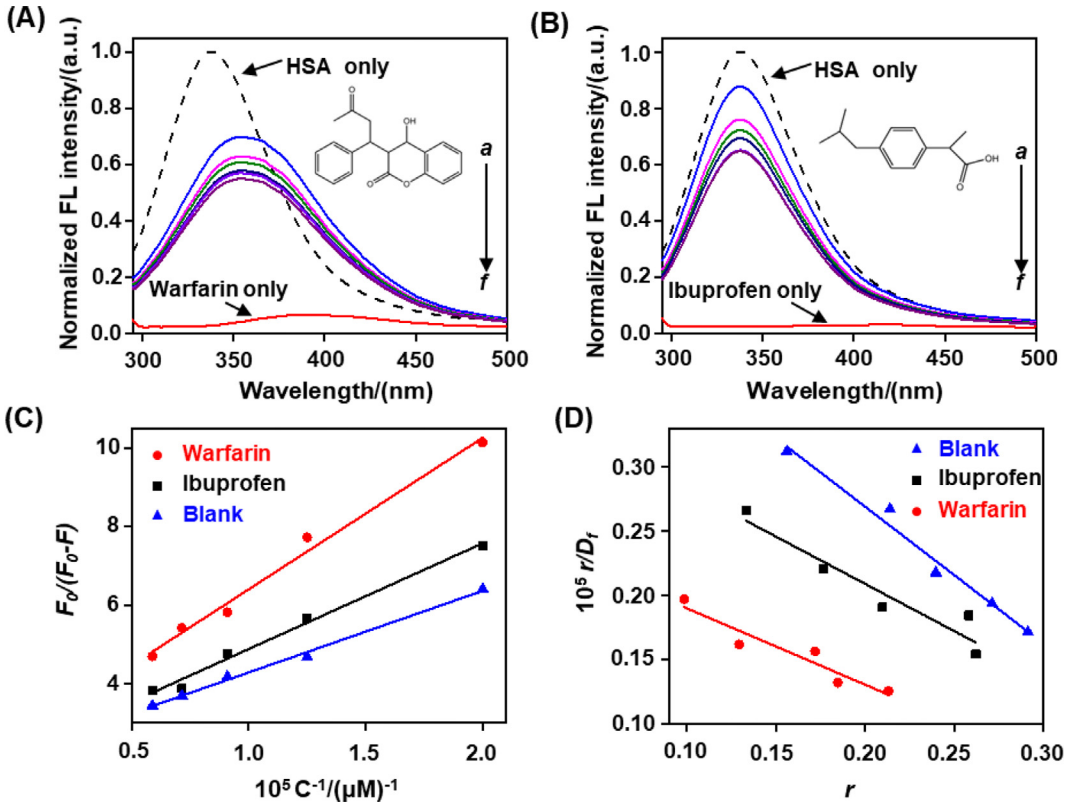

Fig. 7. (A & B) Effects of site marker (*i.e.* warfarin & ibuprofen) to the interaction of HSA-**XB-1** system in PBS buffer (pH = 7.4, 10.0 mM). T = 300 K, λ_{ex} = 280 nm; The concentrations of HSA, warfarin and ibuprofen were 10.0 μM. The curves from (*a*) to (*f*) were indicated the concentration of **XB-1** at 0.0, 5.0, 8.0, 11.0, 14.0, and 17.0 μM, respectively. The insets assigned to the molecular structures of the site marker (A) warfarin and (B) ibuprofen. (C) Modified Stern-Volmer plots and (D) Scatchard plots of the site marker competitive experiments of HSA-**XB-1** system.

Table 3
The binding constants of competitive experiments for HSA-**XB-1** system in PBS buffer (pH = 7.4, 10.0 mM).

Site marker	Modified Stern-Volmer Method			Scatchard Method		
	10^5 K_a (L/mol)	r^a	*S.D.*[b]	10^5 K_b (L/mol)	r^a	*S.D.*[b]
Blank	1.056	0.9978	0.08041	1.067	0.9896	0.08952
Ibuprofen	0.808	0.9951	0.15554	0.736	0.9545	0.13276
Warfarin	0.656	0.9941	0.24312	0.595	0.9517	0.11084

[a] *r* expressed the correlation coefficient.
[b] *S.D.* expressed the standard deviation.

ground-state HSA-**XB-1** complex. In this case, we could calculate the energy transfer efficiency (*E*) through the following empirical formula:

$$E = 1 - \frac{F}{F_0} = \frac{R_0^6}{R_0^6 + r_0^6} \tag{6}$$

where *r* expressed the average distances between Trp residues and **XB-1**, and R_0 corresponded to the critical distance at *E* = 50%, which could be determined with the following empirical formula:

$$R_0^6 = 8.79 \times 10^{-25} K^2 n^{-4} \phi J \tag{7}$$

where K^2 expressed the orientation factor that was associated with internal Trp residuals' geometry as well as the energy acceptor **XB-1**'s dipoles. In fluid solutions, the value of K^2 = 2/3 implied the random orientation. In addition, Ø indicated the Trp residuals' fluorescence quantum yield inside HSA, and *J* assigned to the spectral overlap efficiency between Trp residuals' fluorescence emission and **XB-1**'s absorption spectra, which could be measured by the following empirical formula:

$$J = \frac{\int_0^\infty F(\lambda)\varepsilon(\lambda)\lambda^4 d\lambda}{\int_0^\infty F(\lambda) d\lambda} \tag{8}$$

For this formula, $F(\lambda)$ indicated the corrected fluorescence emission intensity of HSA in the wavelength range from λ to $\lambda + \Delta\lambda$, and the $\varepsilon(\lambda)$ corresponded to the extinction coefficient of **XB-1** at the indicated λ.

According to the primary analysis above, under our experimental conditions, the values of n and Ø values could be considered as ~1.336 and ~0.118, respectively [42]. In this circumstances, the Eqs. (6)–(8) were utilized to calculate the related parameters including $J = 1.5323 \times 10^{-13}$ $cm^3 \cdot L \cdot mol^{-1}$; *E* = 0.2729; R_0 = 3.8635 nm and the binding distance *r* = 4.5489 nm. Notably, both the values of *r* and R_0 were located at the scope among 1–10 nm scale, as well as $0.5R_0 < r < 1.5R_0$, further verifying the energy transfer process from HSA internal Trp residuals to **XB-1**, which agreed well with the static fluorescence quenching principle [28].

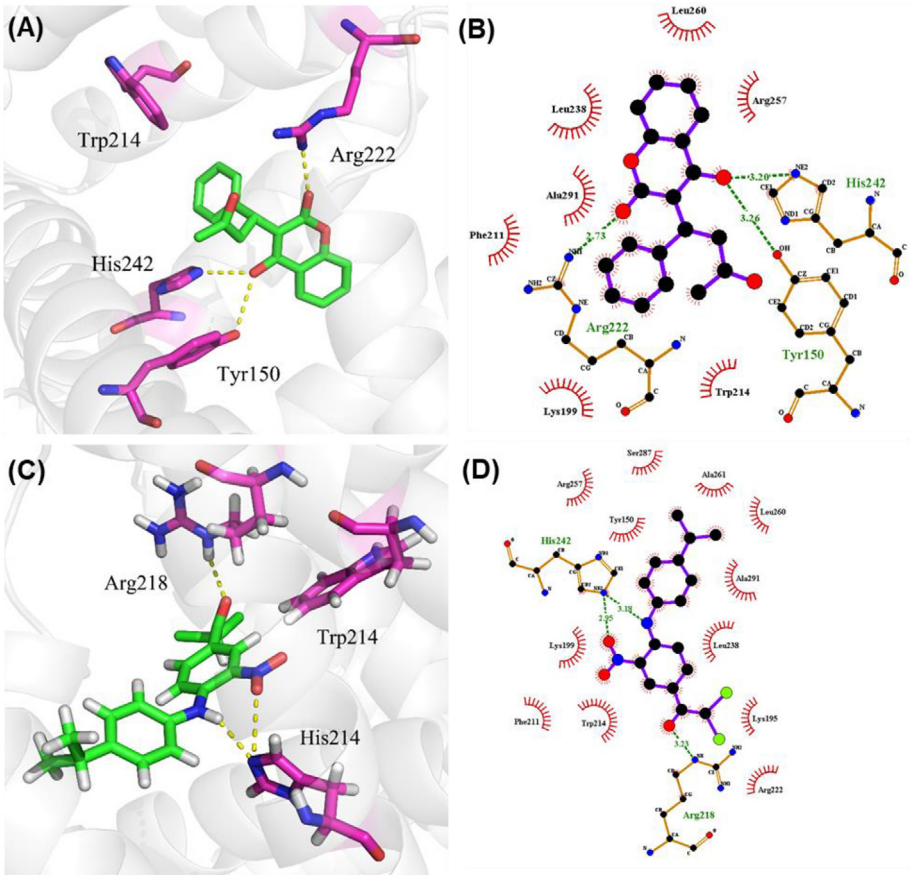

Fig. 8. Binding model of **XB-1** with HSA. (A) 3D diagram of warfarin-HSA complex (PDB code: 2BXD). The yellow dashes represent the hydrogen bond interactions, and the amino acids involved in hydrogen bond interactions were shown as stick and colored as red, the graphics of 3D views were drawn by PyMOL; (B) 2D diagram of hydrogen-bond interaction pattern and hydrophobic contacts between warfarin and HSA. The plots were generated by LigPlot^{+}, hydrogen bonds are shown as green dotted lines, while the spoked arcs represent residues making non-bonded contacts with the ligand; (C) 3D diagram of HSA-**XB-1** complex; (D) 2D diagram of hydrogen-bond interaction pattern and hydrophobic contacts between **XB-1** and HSA.

3.7. Effect of XB-1 on the secondary structure of HSA

In order to demonstrate the effect of **XB-1** on the secondary structure of HSA, the CD spectra of HSA before and after incubation with **XB-1** in aqueous solution (PBS, 10.0 mM, pH = 7.4) were adopted. The results showed that two obvious negative peaks at ~208 nm and ~222 nm were mainly ascribed to the α-helical structure of HSA, which could be effectively reduced by **XB-1**, indicating the conformation alteration of HSA secondary structure caused by **XB-1** (Fig. S6). Based on this fact, the mean residue ellipticities (MRE) for HSA before and after incubation with XB-1 were calculated by the following equation [37]:

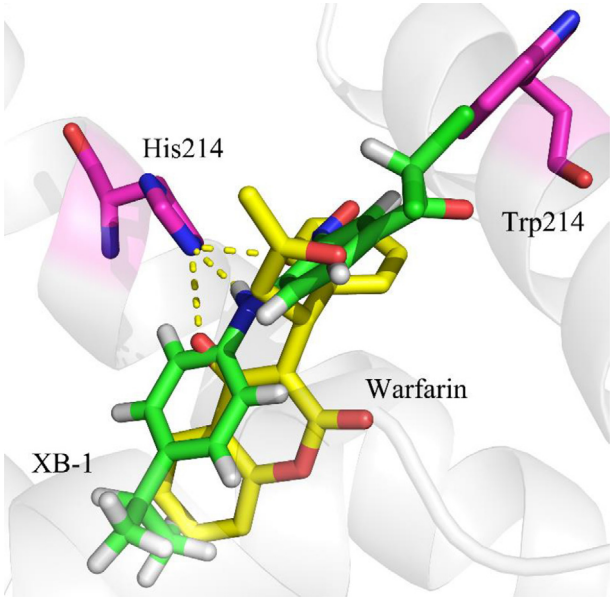

Fig. 9. Overlapping of **XB-1** and warfarin in HSA binding pocket.

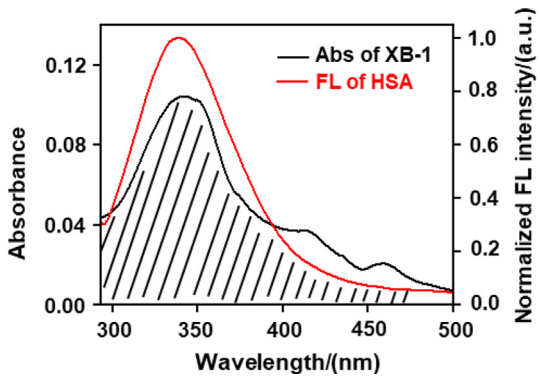

Fig. 10. Efficient spectral overlap of HSA's fluorescence emission with **XB-1**'s absorption spectra in PBS buffer (pH = 7.4, 10.0 mM). T = 300 K, λ_{ex} = 280 nm; Both the concentrations of HSA and **XB-1** were fixed as 10.0 μM.

$$MRE = \frac{ObservedCD(mdeg)}{C_p \times n \times l \times 10} \quad (9)$$

In this expression, C_p = 20.0 μM showed the molar concentration of HSA; n = 585 expressed the amino acid residues number; l = 1.0 cm expressed the path length.

Afterward, the contents of α-helix in HSA in the absence and presence of **XB-1** were further measured by exploiting the MRE values at 208 nm (MRE_{208}) to the following equation [20]:

$$\alpha - helix(\%) = \frac{-MRE_{208} - 4000}{33,000 - 4000} \times 100 \quad (10)$$

The results showed that the α-helix contents of HSA in the absence and presence of **XB-1** were 48.6% and 36.0%, implying a noticeable loss of α-helix in HSA caused by **XB-1** [6].

4. Conclusions

In summary, the binding of a novel PDK inhibitor **XB-1** to HSA was firstly demonstrated using spectroscopic approaches and molecular docking under simulative physiological conditions (PBS, pH = 7.4, 10.0 mM). This work displayed that IFE played an important role in the intrinsic fluorescence quenching of HAS caused by **XB-1.** After excluding the IFE process, the corrected fluorescence of HSA could be also quenched by **XB-1**, which was attributable to the static quenching mechanism. In addition, the site marker competitive experiments and molecular docking clearly revealed that **XB-1** primary bound to the site I of HSA mainly through hydrogen bond interaction. We envision that this work will offer significant information for understanding the potential biological toxicity of **XB-1** *in vivo*, which could be helpful for us to guide the reasonable clinical application of **XB-1** during human against diseases.

CRediT authorship contribution statement

Xianjiu Liao: Conceptualization, Formal analysis, Writing - original draft, Funding acquisition. **Chunlei Zhu:** Data curation, Formal analysis. **Ding Huang:** Data curation. **Xiaoqing Wen:** Writing - original draft. **Shao-Lin Zhang:** Conceptualization, Writing - review & editing, Funding acquisition. **Yizhong Shen:** Conceptualization, Writing - review & editing, Funding acquisition.

Declaration of Competing Interest

The authors declare that they have no known competing financial interests or personal relationships that could have appeared to influence the work reported in this paper.

Acknowledgements

This work was supported by the National Natural Science Foundation of China (21804029, 21807008, 21964018), the distinguished Young Talents of Youjiang Medical University for Nationalities, the Natural Science Foundation of Guangxi Province (2018GXNSFAA138211), Research Program of Baise Science and Technology Development Plan (20201739), and the subject academic team of Youjiang Medical University for Nationalities (Pharmaceutical analysis).

Appendix A. Supplementary material

Supplementary data to this article can be found online at https://doi.org/10.1016/j.saa.2021.119733.

References

[1] E. Mrkalic, R. Jelic, S. Stojanovic, M. Sovrlic, Interaction between olanzapine and human serum albumin and effect of metal ions, caffeine and flavonoids on the binding: A spectroscopic study, Spectrochim. Acta, Part A 249 (2021) 119295.
[2] M. Kooravand, S. Asadpour, H. Haddadi, S. Farhadian, An insight into the interaction between malachite green oxalate with human serum albumin: Molecular dynamic simulation and spectroscopic approaches, J. Hazard. Mater. 407 (2021) 124878.
[3] H. Chen, C. Zhu, F. Chen, J. Xu, X. Jiang, Z. Wu, X. Ding, G.-C. Fan, Y. Shen, Y. Ye, Profiling the interaction of Al(III)-GFLX complex, a potential pollution risk, with bovine serum albumin, Food Chem. Toxicol. 136 (2020) 111058.
[4] O. Mazuryk, P. Gajda-Morszewski, M. Flejszar, P. Labuz, R. van Eldik, G. Stochel, M. Brindell, Influence of aqueous extracts of urban airborne particulate matter on the structure and function of human serum albumin, Environ. Pollut. 263 (2020) 114667.
[5] S. Seyedi, P. Parvin, A. Jafargholi, S. Jelvani, M. Shahabi, M. Shahbazi, P. Mohammadimatin, A. Moafi, Fluorescence properties of Phycocyanin and Phycocyanin-human serum albumin complex, Spectrochim. Acta, Part A 239 (2020) 118468.
[6] Y. Shen, C. Zhu, Y. Wang, J. Xu, R. Xue, F. Ji, Y. Wu, Z. Wu, W. Zhang, Z. Zheng, Y. Ye, Evaluation the binding of chelerythrine, a potentially harmful toxin, with bovine serum albumin, Food Chem. Toxicol. 135 (2020) 110933.
[7] Z. Faisal, V. Voros, E. Fliszar-Nyul, B. Lemli, S. Kunsagi-Mate, R. Csepregi, T. Koszegi, F. Zsila, M. Poor, Probing the Interactions of Ochratoxin B, Ochratoxin C, Patulin, Deoxynivalenol, and T-2 Toxin with human serum albumin, Toxins 12 (2020) 12060392.
[8] Z. Preisz, S. Kunsagi-Mate, Effect of methotrexate and its photodegradation products on the temperature induced denaturation of human serum albumin, Spectrochim. Acta, Part A 245 (2021) 118905.
[9] F. Shiri, S. Shahraki, M. Bazzi-Alahri, Assessing the in vitro and in silico interactions of two Palladium(II) dithiocarbamate complexes with human serum albumin, J. Mol. Struct. 1221 (2020) 128809.
[10] N. Shahabadi, M. Falsafi, S. Hadidi, Molecular modeling and multispectroscopic studies of the interaction of hepatitis B drug, adefovir dipivoxil with human serum albumin, J. Lumin. 167 (2015) 339–346.
[11] T.A. Wani, A.H. Bakheit, S. Zargar, Z.S. Alanazi, A.A. Al-Majed, Influence of antioxidant flavonoids quercetin and rutin on the in-vitro binding of neratinib to human serum albumin, Spectrochim. Acta, Part A 246 (2021) 118977.
[12] N. Cacita, S. Nikolaou, Studying the interaction between trinuclear ruthenium complexes and human serum albumin by means of fluorescence quenching, J. Lumin. 169 (2016) 115–120.
[13] S. Sekowski, M. Bitiucki, M. Ionov, M. Zdeb, N. Abdulladjanova, R. Rakhimov, S. Mavlyanov, M. Bryszewska, M. Zamaraeva, Influence of valoneoyl groups on the interactions between Euphorbia tannins and human serum albumin, J. Lumin. 194 (2018) 170–178.
[14] M. Steblecka, M. Wolszczak, E. Szajdzinska-Pietek, Interaction of 1-pyrene sulfonic acid sodium salt with human serum albumin, J. Lumin. 172 (2016) 279–285.
[15] M. Tanaka, Y. Asahi, S. Masuda, Interaction between drugs and water-soluble polymers. VII. binding of berberine with bovine serum albumin, J. Macromol. Sci. A 32 (1995) 339–347.
[16] E. Ayranci, O. Duman, Binding of fluoride, bromide and iodide to bovine serum albumin, studied with ion-selective electrodes, Food Chem. 84 (2004) 539–543.
[17] E. Ayranci, O. Duman, Binding of lead ion to bovine serum albumin studied by ion selective electrode, Protein Peptide Lett. 11 (2004) 331–337.
[18] S. Tunc, O. Duman, B.K. Bozoglan, Studies on the interactions of chloroquine diphosphate and phenelzine sulfate drugs with human serum albumin and human hemoglobin proteins by spectroscopic techniques, J. Lumin. 140 (2013) 87–94.
[19] J.H. Tang, F. Luan, X.G. Chen, Binding analysis of glycyrrhetinic acid to human serum albumin: Fluorescence spectroscopy, FTIR, and molecular modeling, Bioorg. Med. Chem. Lett. 14 (2006) 3210–3217.
[20] B.K. Bozoglan, S. Tunc, O. Duman, Investigation of neohesperidin dihydrochalcone binding to human serum albumin by spectroscopic methods, J. Lumin. 155 (2014) 198–204.
[21] O. Duman, S. Tunc, B.K. Bozoglan, Characterization of the binding of metoprolol tartrate and guaifenesin drugs to human serum albumin and human hemoglobin proteins by fluorescence and circular dichroism spectroscopy, J. Fluorescenc. 23 (2013) 659–669.
[22] S. Tunc, O. Duman, I. Soylu, B.K. Bozoglan, Spectroscopic investigation of the interactions of carbofuran and amitrol herbicides with human serum albumin, J. Lumin. 151 (2014) 22–28.
[23] S.-L. Zhang, Y. He, K.Y. Tam, Targeting cancer metabolism to develop human lactate dehydrogenase (hLDH)5 inhibitors, Drug Discov. Today 23 (2018) 1407–1415.
[24] S.-L. Zhang, Z. Yang, X. Hu, H. Chakravarty, K.Y. Tam, Anticancer effects of some novel dichloroacetophenones through the inhibition of pyruvate dehydrogenase kinase 1, Eur. J. Pharm. Sci. 123 (2018) 43–55.
[25] F. Liu, Y. Zhang, Q. Yu, Y. Shen, Z. Zheng, J. Cheng, W. Zhang, Y. Ye, Exploration of the binding between ellagic acid, a potentially risky food additive, and bovine serum albumin, Food Chem. Toxicol. 134 (2019) 110867.

[26] D. Lu, X. Zhao, Y. Zhao, B. Zhang, B. Zhang, M. Geng, R. Liu, Binding of Sudan II and Sudan IV to bovine serum albumin: Comparison studies, Food Chem. Toxicol. 49 (2011) 3158–3164.
[27] B. Yang, F. Hao, J. Li, K. Wei, W. Wang, R. Liu, Characterization of the binding of chrysoidine, an illegal food additive to bovine serum albumin, Food Chem. Toxicol. 65 (2014) 227–232.
[28] D. Zhang, X. Zhang, Y.-C. Liu, S.-C. Huang, Y. Ouyang, Y.-J. Hu, Investigations of the molecular interactions between nisoldipine and human serum albumin in vitro using multi-spectroscopy, electrochemistry and docking studies, J. Mol. Liq. 258 (2018) 155–162.
[29] M.S. Ali, H.A. Al-Lohedan, Spectroscopic and molecular docking investigation on the noncovalent interaction of iysozyme with saffron constituent "safranal", ACS Omega 5 (2020) 9131–9141.
[30] M.S. Ali, J. Muthukumaran, H.A. Al-Lohedan, Molecular interactions of ceftazidime with bovine serum albumin: Spectroscopic, molecular docking, and DFT analyses, J. Mol. Liq. 313 (2020) 113490.
[31] R. Mi, Y.-J. Hu, X.-Y. Fan, Y. Ouyang, A.-M. Bai, Exploring the site-selective binding of jatrorrhizine to human serum albumin: Spectroscopic and molecular modeling approaches, Spectrochim. Acta, Part A 117 (2014) 163–169.
[32] M.S. Ali, M. Amina, H.A. Al-Lohedan, N.M. Al Musayeib, Human serum albumin binding to the biologically active labdane diterpene "leoheterin": Spectroscopic and in silico analysis, J. Photoch. Photobiol. B 182 (2018) 9–17.
[33] M.S. Ali, H.A. Al-Lohedan, Deciphering the interaction of procaine with bovine serum albumin and elucidation of binding site: A multi spectroscopic and molecular docking study, J. Mol. Liq. 236 (2017) 232–240.
[34] M. Beg, A. Maji, A.K. Mandal, S. Das, P.K. Jha, M. Hossain, Probing the binding of Spathodea campanulata leaves extract mediated biogenic potential microbicidal silver nanoparticles to human serum albumin: An insight in the light of spectroscopic approach, J. Lumin. 202 (2018) 147–156.
[35] A. Szkudlarek, A. Sulkowska, M. Maciazek-Jurczyk, M. Chudzik, J. Rownicka-Zubik, Effects of non-enzymatic glycation in human serum albumin. Spectroscopic analysis, Spectrochim. Acta, Part A 152 (2016) 645–653.
[36] M.S. Ali, H.A. Al-Lohedan, Experimental and computational investigation on the molecular interactions of safranal with bovine serum albumin: Binding and anti-amyloidogenic efficacy of ligand, J. Mol. Liq. 278 (2019) 385–393.
[37] M.S. Ali, H.A. Al-Lohedan, Spectroscopic and computational evaluation on the binding of safranal with human serum albumin: Role of inner filter effect in fluorescence spectral correction, Spectrochim. Acta, Part A 203 (2018) 434–442.
[38] Y. Ye, T. Wu, X. Jiang, J. Cao, X. Ling, Q. Mei, H. Chen, D. Han, J.-J. Xu, Y. Shen, Portable smartphone-based QDs for the visual onsite monitoring of fluoroquinolone antibiotics in actual food and environmental samples, ACS Appl. Mater. Interfaces 12 (2020) 14552–14562.
[39] B. Tu, Y. Wang, R. Mi, Y. Ouyang, Y.-J. Hu, Evaluation of the interaction between naringenin and human serum albumin: Insights from fluorescence spectroscopy, electrochemical measurement and molecular docking, Spectrochim. Acta, Part A 149 (2015) 536–543.
[40] P.D. Ross, S. Subramanian, Thermodynamics of protein association reactions: forces contributing to stability, Biochemistry 20 (1981) 3096–3102.
[41] S.-L. Zhang, H. Yao, C. Wang, K.Y. Tam, Study the interactions between human serum albumin and two antifungal drugs: Fluconazole and its analogue DTP, Bioorg. Med. Chem. Lett. 24 (2014) 4963–4968.
[42] G. Zhang, L. Wang, J. Pan, Probing the Binding of the Flavonoid Diosmetin to Human Serum Albumin by Multispectroscopic Techniques, J. Agric. Food. Chem. 60 (2012) 2721–2729.